CORRELATION OF SMART ACTIVE FLAP ROTOR LOADS

Sesi Kottapalli
Flight Vehicle Research and Technology Division
NASA Ames Research Center
Moffett Field, California
Sesi.B.Kottapalli@nasa.gov

and

Friedrich Straub
The Boeing Company
Mesa, Arizona
friedrich.k.straub@boeing.com

The ability to predict SMART active trailing edge flap rotor loads is explored in this study. Full-scale wind tunnel data recently acquired in the NASA Ames 40- by 80- Foot Wind Tunnel are compared with analytical results from CAMRAD II. For the 5-bladed rotor, two high-speed forward flight cases are considered, namely, a 0 deg flap deflection case and a 5P, 2 deg flap deflection case. Overall, the correlation is reasonable, with the following exceptions: the torsion moment frequency and the chordwise bending moment are underpredicted. In general, the effect of the 5P, 2 deg flap motion is captured by the analysis, though there is overprediction in the neighborhood of the 105 deg and 120 deg azimuthal locations. Changes to the flexbeam torsion stiffness are also briefly considered in this study, as this stiffness will be updated in the future. Finally, the indication is that compressibility effects are important, and this suggests that computational fluid dynamics might improve the current correlation.

Notation

C_T	Helicopter thrust coefficient
DTEF	Flap hinge damping, ft-lb/rad/sec
KTEF	Flap hinge stiffness, ft-lb/rad
MTEF	Flap mass, slug
NP	Integer (N) multiple of rotor speed
per/ rev	Per revolution
α_s	Rotor shaft angle
μ	Rotor advance ratio
σ	Rotor solidity ratio

Introduction

DARPA, Boeing, and NASA have recently completed a successful, full-scale wind tunnel test of the Boeing Smart Material Advanced Rotor Technology (SMART) rotor, Refs. 1 and 2. The data from this wind tunnel test will be used to validate the Helicopter Quieting Program noise prediction tools as well as to improve NASA's ability to predict rotor performance, vibration, and loads. The SMART rotor is a next generation rotor system that offers high bandwidth on-blade active trailing edge flaps, which will provide unique modeling challenges for the vibration and noise prediction tool sets. Reference 3 contains a description of the SMART rotor. The present work is a companion study to Refs. 1 and 2, and focuses on the correlation of the rotor loads.

The overall objective of the present correlation study is to establish the best comprehensive analysis model of the SMART rotor to be used as a vibration and loads prediction tool. The short-term program goal is to use the analytical model for pre-flight predictions prior to the planned, future flight test of the SMART rotor. The ultimate goal of this effort is to provide the blade designer with a reliable predictive tool that can lead to optimized blades and on-blade controls, with reductions in the money and time spent on wind tunnel and flight tests.

The basic rotor without the smart material technology is derived from the five-bladed MD 900 Explorer main rotor. It has a radius of 16.9 ft and a nominal 1g thrust of approximately 6,000 lbs, Ref. 3 and 4. References 5-7 describe the 1992 wind tunnel test conducted at NASA Ames with the MDART rotor, a pre-production version of the Explorer rotor. The blades and flexbeams are made of fiberglass and the pitchcase, for which high stiffness is essential, is made of graphite. The flexbeam extends to approximately 0.20R. The implementation of the smart material active trailing edge flaps is described in Refs. 1 and 3. The SMART rotor trailing edge flap extends from approximately 0.75R to 0.92R, Ref. 1.

The present study considers the first step in the prediction of the five-bladed SMART rotor loads. The rotor loads include the blade loads and the pitch link loads. In this study, a fixed, rigid hub is considered, i.e., the fuselage effects are not included. The effects of the individual trailing edge flaps on the rotor loads are considered by studying the following two cases: first, a 0 deg flap deflection case and second, a 2 deg flap

Presented at the American Helicopter Society 65th Annual Forum, Grapevine, TX, May 27-29, 2009.

deflection at 5P case. The rotorcraft comprehensive analysis CAMRAD II (Refs. 8-10) is used to model the SMART rotor.

Analytical Model

The CAMRAD II analytical model used in the current correlation study is briefly described as follows. The SMART rotor blade and flexbeam are modeled using elastic beam elements, with each element having two elastic flap bending, two elastic lag bending, and two torsion degrees of freedom. The blade consists of four beam elements, the torque tube one element, and the flexbeam three elastic elements (plus a rigid element at each end of the flexbeam). The trailing edge flap was modeled as a rigid body, using the measured flap hinge stiffness, flap hinge damping, and flap mass. The flap extends from 0.74R to 0.92R. The aerodynamic model used 20 spanwise panels for the entire blade, 10 inboard of the flap, 6 on the flap (from 0.74R to 0.92R), and 4 outboard of the flap. A rolled up wake model, with single tip vortex and single circulation peak, has been used, including free wake geometry.

Measured Wind Tunnel Data

References 1 and 2 contain descriptions of the recent SMART Rotor test in the NASA Ames 40- by 80- Foot Wind Tunnel. The wind tunnel data used in the current paper is taken from Ref. 1.

Results

The results in this paper are given for the following operating condition: $\mu = 0.3$, $C_T/\sigma = 0.08$, $\alpha_s = -9.1$ deg. The following two cases are considered: 0 deg flap deflection and 2 deg trailing edge flap deflection (90 deg phase) at 5P.

The predicted hover torsion frequency, including the flap mass and inertia, is 5.8P, and this has been obtained with a value of the pitch link stiffness of 114,000 lb/ft. During the wind tunnel test, the measured torsion frequency was 5.85P (Ref. 1). Since the above analytical and experimental hover torsion frequencies are sufficiently close to each other, the pitch link stiffness was kept unchanged at its current value throughout this study. Finally, the measured time histories shown in this paper have been obtained using the first eight harmonics of the test data.

Methodology Details

The overall, stepwise procedure to get a converged, trimmed CAMRAD II run for the SMART rotor is outlined as follows: first, the advance ratio is increased from the hover condition to its final value, 0.3; and second, the 5P flap deflection is incrementally increased from 0 deg to the final 2 deg. A small amount of structural damping has been introduced to ensure convergence.

First Pass Correlation

This section summarizes the first pass correlation attempt for the 0 deg flap deflection case. The first set of the results is shown in Figs. 1a-1f. The measured and the first pass, predicted blade torsion moments are shown in Figs. 1a-1b, at 0.64R and 0.81R, respectively. The corresponding flatwise and chordwise bending moment correlations are shown in Figs. 1c-1f, at 0.59R and 0.81R, respectively. Overall, the correlation is less than satisfactory, Figs. 1a-1d. For example, Figs. 1a-1b show two types of discrepancies between the measured and the analytical torsion moments, as follows: first, the analysis overpredicts the advancing blade dip, 90 deg to 120 deg azimuth, and second, overall, the analysis underpredicts the waveform frequency, seen clearly between 150 deg to 360 deg azimuth. The analysis also overpredicts the advancing blade dip for the flatwise bending moments, Figs. 1c-1d. The following briefly describes additional efforts to improve the above correlation.

A parametric study has been conducted in which the following trailing edge flap properties have been varied: the trailing edge flap hinge spring stiffness, KTEF, the flap hinge damping, DTEF, and the flap mass, MTEF. Figures 2a-2f show the effect of changing the flap hinge stiffness KTEF from its baseline value ("Bsln KTEF") to twice its baseline value ("2.0X KTEF"), with all other parameters kept at their baseline values. The analysis predicts that a flap hinge stiffness of 1.5X the baseline value gives the best match with the measurements, Figs. 2a-2d. Figures 2g-2h show that the flap hinge damping DTEF does not have any significant effect. Finally, Fig. 2i shows, as a sample, that the flap mass MTEF has a significant effect on the blade torsion moment. However, at present it has been determined that there is little uncertainty in the baseline flap properties as currently modeled, and consequently, the above line of investigation, varying the trailing edge flap properties, was terminated.

For the current high-speed operating condition of interest, the advancing blade tip Mach number is 0.81, and thus the effect of compressibility on the SMART rotor loads should be considered. A compressibility related parametric variation has been conducted, and it has been found that to get the best correlation for the torsion and the flatwise blade loads, it is necessary to introduce an analytical Mach number correction factor. By definition, the effective Mach number = (correction factor) * Mach number, with a default correction factor = 1. It has also been found that it is necessary to correct

only the airfoil pitching moment Mach number, and that by a small amount, i.e., the pitching moment effective Mach number correction factor = 0.92. This correction is needed only in the blade tip region, 0.74R to the tip. Overall, a Mach number correction factor < 1 is just an indication of the importance of compressibility, and suggests that computational fluid dynamics, CFD, might improve the correlation. All of the following analytical results in this paper have been obtained using an airfoil pitching moment Mach number correction factor = 0.92, with all of the blade and flap properties kept unchanged at their baseline values as currently modeled.

Blade Frequencies and Control Angles

Table 1 shows the CAMRAD II SMART rotor blade frequencies. Table 2 shows the measured and calculated control angles required for trim, and these are in reasonable agreement.

Blade Loads Correlation, 0 deg Flap Deflection

Blade Moments. This group of results, Figs. 3a-3f, shows the measured and the predicted blade torsion moments, and the flatwise and chordwise bending moments (mean removed) for the 0 deg flap deflection case. Overall, the correlation is reasonable, and the analysis captures almost all of the basic features of the measured waveforms, Figs. 3a-3f, with the exceptions noted as follows. For the torsion moments, Figs. 3a-3b, the forced response analytical frequency is lower than the experimental frequency. In the analysis, the blade pitch link stiffness has been varied to see if the above frequency is sensitive to the pitch link stiffness, and it was found that this is not so. Also, Figs. 3e-3f show that there is some underprediction of the chordwise bending moments.

Pitch Link Loads. Figure 4 shows the correlation for the pitch link load time history (mean removed) for the 0 deg flap deflection case. The corresponding cyclic (half peak to peak) pitch link loads are as follows: analysis, 75 lb, and test, 93 lb. Overall, the pitch link load correlation is reasonable.

Blade Loads Correlation, 2 deg Flap Deflection (90 deg phase) at 5P

Blade Moments. This group of results, Figs. 5a-5f, shows the measured and the predicted blade torsion moments, and the flatwise and chordwise bending moments (mean removed) for the 5P, 2 deg flap deflection case. Overall, the correlation is reasonable, Figs. 5a-5f, though there is overprediction in the neighborhood of the 105 deg and 120 deg azimuthal locations, Figs. 5a-5d. Also, the chordwise bending moments are underpredicted, Figs. 5e-5f.

Pitch Link Loads. Figure 6 shows the correlation for the pitch link load time history (mean removed) for the 5P, 2 deg flap deflection case. The corresponding cyclic (half peak to peak) pitch link loads are as follows: analysis, 193 lb, and test, 191 lb. The analysis overpredicts the dip in the neighborhood of the 120 deg azimuthal location, Fig. 6. Overall, the pitch link load correlation is reasonable,

Analytical Effect of Flexbeam Torsion Stiffness

Since over the years the original MD 900 Explorer flexbeam has undergone several changes prior to its specific use in the SMART rotor wind tunnel test, an analytical study has been conducted in which only the flexbeam torsion stiffness has been varied (baseline to 8X the baseline torsion stiffness). It is planned that in the near future Boeing, Mesa, will conduct an experimental investigation to measure the SMART rotor flexbeam torsion stiffness.

Since the flexbeam is very soft in torsion compared to the pitchcase, even an 8X increase in the flexbeam torsion stiffness does not significantly change the blade torsion frequency (the change is less than 0.2%). However, the pitch link load is affected by the change in the flexbeam torsion stiffness, and this can be seen from Fig. 7 that shows the predicted cyclic pitch link load versus the flexbeam torsion stiffness, for both the 0 deg and 5P, 2 deg flap deflection cases. Overall, from the 0 deg flap deflection prediction shown in Fig. 7, it appears that the actual SMART rotor flexbeam torsion stiffness may be roughly 4X to 6X the baseline value used in this study. Finally, the analytical results showed that the fixed system 5P hub loads are not sensitive to changes in the flexbeam torsion stiffness.

Conclusions

The prediction of the SMART active trailing edge flap rotor loads was considered in this analytical study. The following two cases were considered: 0 deg flap deflection and 2 deg trailing edge flap deflection (90 deg phase) at 5P. Reasonable correlation was obtained with recently measured full-scale wind tunnel data. The indication is that compressibility effects are important, and this suggests that computational fluid dynamics, CFD, might improve the current correlation. Specific conclusions are as follows:

1. For the 0 deg flap deflection case, the torsion moment and the flatwise bending moment were predicted reasonably well. The frequency of the torsion moment was underpredicted.

For the 5P, 2 deg flap case, the effect of the flap motion was reasonably captured, though there was overprediction in the neighborhood of the 105 deg and 120 deg azimuthal locations,

The pitch link load was reasonably predicted for the two operating conditions that were considered.

2. The chordwise bending moment was predicted reasonably well, except that the overall magnitude was underpredicted.

3. The analytical study involving the flexbeam torsion stiffness showed that the actual flexbeam torsion stiffness may be roughly 4X to 6X the baseline value used in this study.

References

1. Straub, F. K., Anand, V. R., Birchette, T. S., and Lau, B. H., "Wind Tunnel Test of the SMART Active Flap Rotor," American Helicopter Society 65th Annual Forum Proceedings, Grapevine, TX, May 27-29, 2009.

2. Straub, F. K, Anand, V. R., Hall, S. R., and Lau, B.H., "Dynamics and Active Flap Control of the SMART Rotor," American Helicopter Society 65th Annual Forum Proceedings, Grapevine, TX, May 27-29, 2009.

3. Straub, F. K. and Anand, V.R., "Whirl Tower Test and Analysis of the Smart Material Actuated Rotor Technology (SMART) Active Flap Rotor," American Helicopter Society 63rd Annual Forum Proceedings, Virginia Beach, VA, May 1-3, 2007.

4. Murrill, R.J., Hamilton, B.K., Anand, V.R., Lauzon, D.M., and Tuttles, B., "Bearingless Main Rotor Whirl Test: Design, Analysis, and Test Results," American Helicopter Society 49th Annual Forum Proceedings, St. Louis, MO, May 19-21, 1993.

5. McNulty, M., Jacklin, S., and Lau, B., "A Full-Scale Test of the McDonnell Douglas Advanced Bearingless Rotor in the NASA Ames 40- by 80- Foot Wind Tunnel," American Helicopter Society 49th Annual Forum Proceedings, St. Louis, MO, May 19-21, 1993.

6. Khanh, K., McNulty, M., Anand, V., and Lauzon, D., "Aeroelastic Stability of the McDonnell Douglas Advanced Bearingless Rotor" American Helicopter Society 49th Annual Forum Proceedings, St. Louis, MO, May 19-21, 1993.

7. Jacklin, S. J., Lau, B. H., Nguyen, K. Q., Smith, R. L., and McNulty, M.J., "Full-Scale Wind Tunnel Test of the McDonnell Douglas Five-Bladed Advanced Bearingless Rotor: Performance, Stability, Loads, Control Power, Vibration and HHC Data," American Helicopter Society, American Helicopter Society Aeromechanics Specialists Conference, San Francisco, CA, January 19-21, 1994.

8. Johnson, W. "CAMRAD II, Comprehensive Analytical Model of Rotorcraft Aerodynamics and Dynamics," Johnson Aeronautics, Palo Alto, California, 1992-1999.

9. Johnson, W. "Technology Drivers in the Development of CAMRAD II," American Helicopter Society, American Helicopter Society Aeromechanics Specialists Conference, San Francisco, CA, January 19-21, 1994.

10. Johnson, W. "A General Free Wake Geometry Calculation for Wings and Rotors," American Helicopter Society 51st Annual Forum Proceedings, Ft. Worth, TX, May 9-11, 1995.

Table 1. Predicted SMART rotor blade frequencies.

Blade Mode	Frequency (Per Rev)
Chord 1	0.564
Flap 1	1.037
Flap 2	2.816
Chord 2	4.411
Flap 3	4.537
Torsion 1	5.797

Table 2. Measured and predicted control angles for trim, $\mu = 0.3$, $C_T/\sigma = 0.08$, $\alpha_s = -9.1$ deg.

	Measured, deg		Predicted, deg	
	0 deg Flap	2 deg Flap	0 deg Flap	2 deg Flap
Collective	10.89	11.15	10.73	10.64
Lateral	-2.61	-2.67	-2.21	-2.15
Longitudinal	6.11	6.11	6.66	6.91

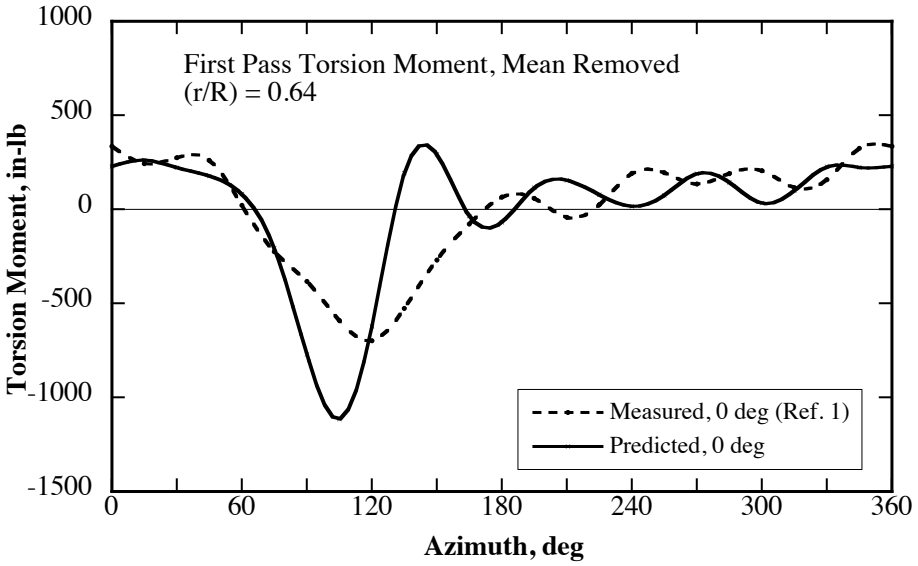

Fig. 1a. Measured wind tunnel and first pass, predicted torsion moments at 0.64R, 0 deg flap , $\mu = 0.3$, $C_T/\sigma = 0.08$, $\alpha_s = -9.1$ deg.

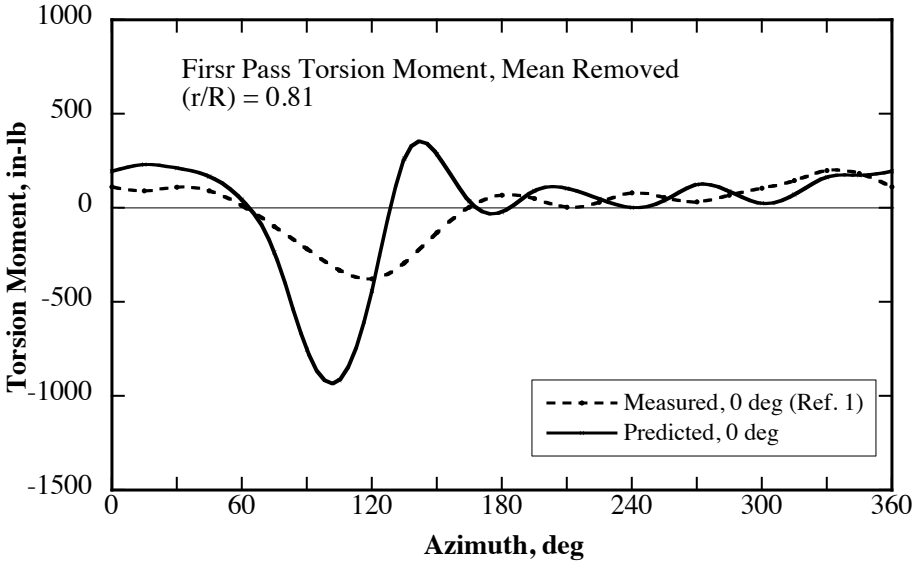

Fig. 1b. Measured wind tunnel and first pass, predicted torsion moments at 0.81R, 0 deg flap, $\mu = 0.3$, $C_T/\sigma = 0.08$, $\alpha_s = -9.1$ deg.

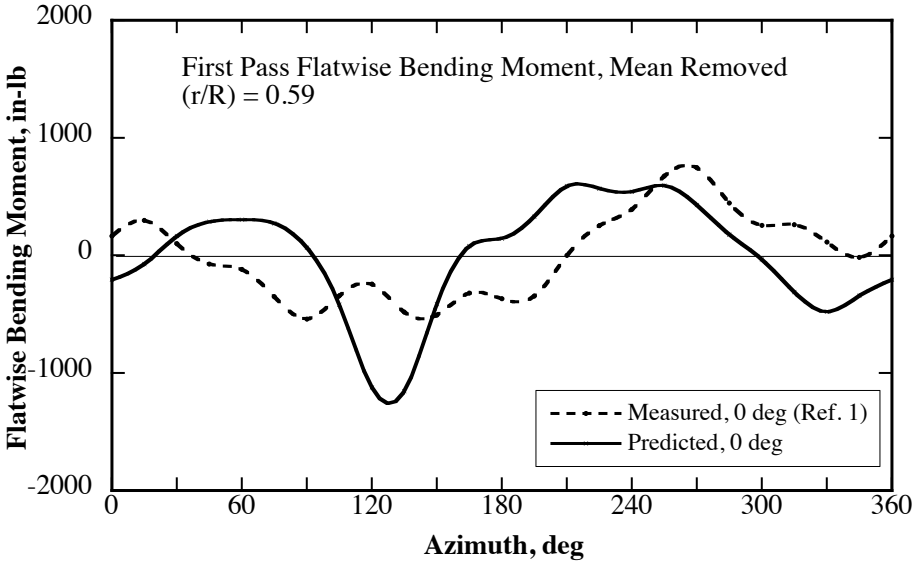

Fig. 1c. Measured wind tunnel and first pass, predicted flatwise bending moments at 0.59R, 0 deg flap, $\mu = 0.3$, $C_T/\sigma = 0.08$, $\alpha_s = -9.1$ deg.

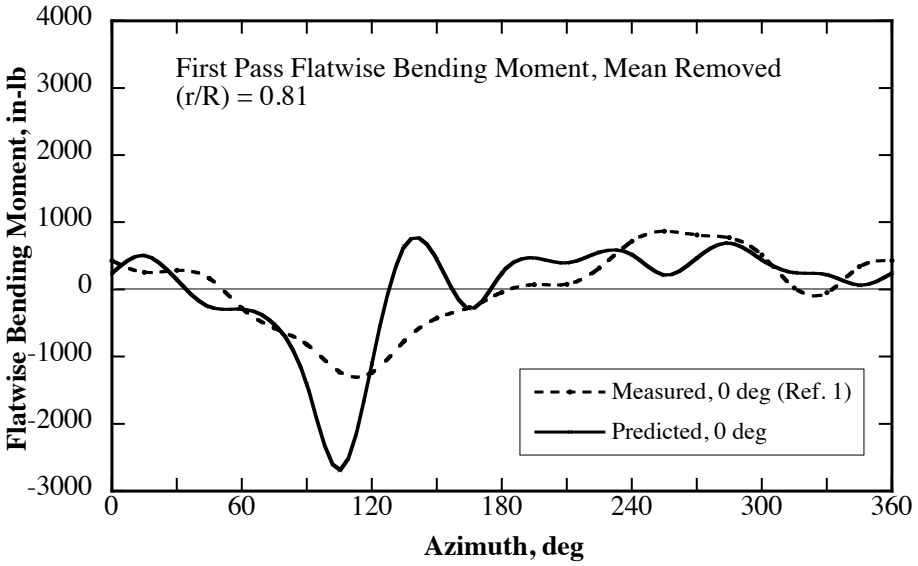

Fig. 1d. Measured wind tunnel and first pass, predicted flatwise bending moments at 0.81R, 0 deg flap, $\mu = 0.3$, $C_T/\sigma = 0.08$, $\alpha_s = -9.1$ deg.

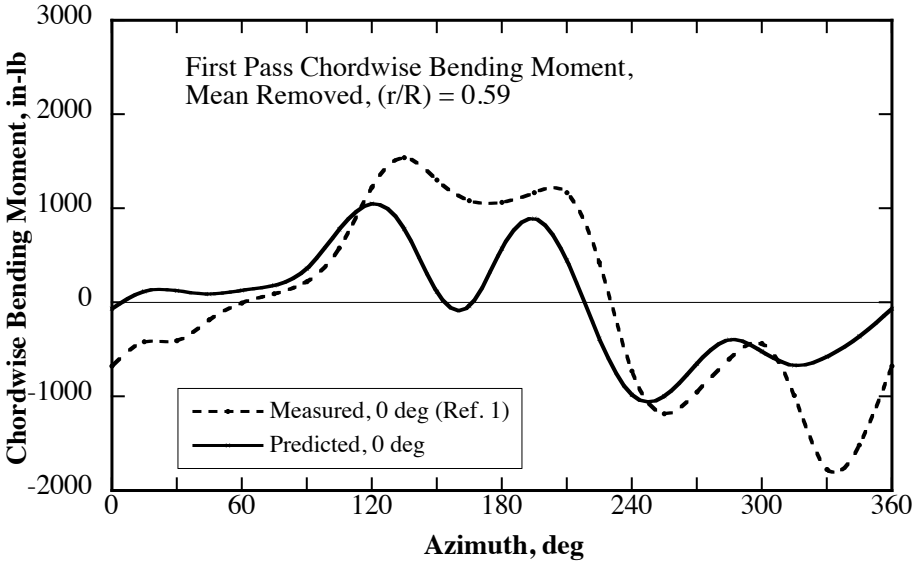

Fig. 1e. Measured wind tunnel and first pass, predicted chordwise bending moments at 0.59R, 0 deg flap, $\mu = 0.3$, $C_T/\sigma = 0.08$, $\alpha_s = -9.1$ deg.

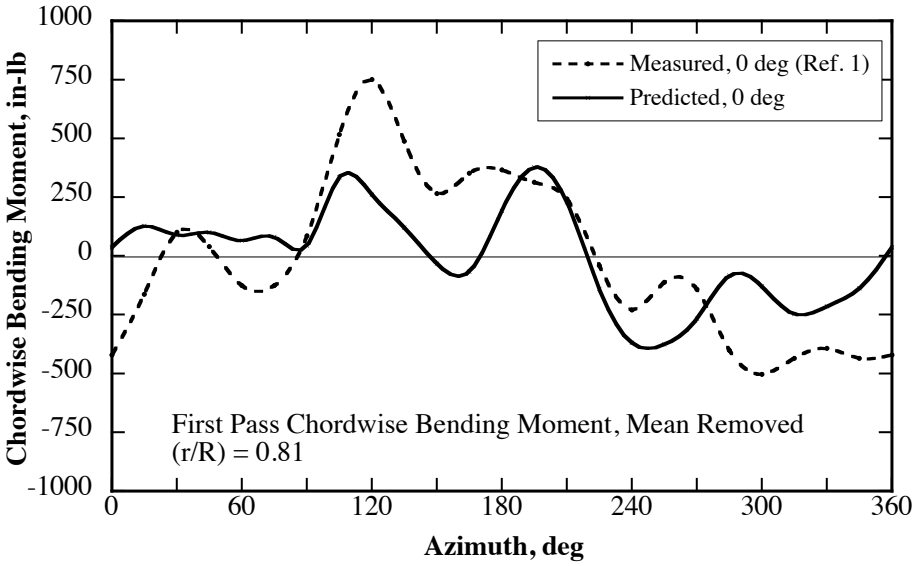

Fig. 1f. Measured wind tunnel and first pass, predicted chordwise bending moments at 0.81R, 0 deg flap, $\mu = 0.3$, $C_T/\sigma = 0.08$, $\alpha_s = -9.1$ deg.

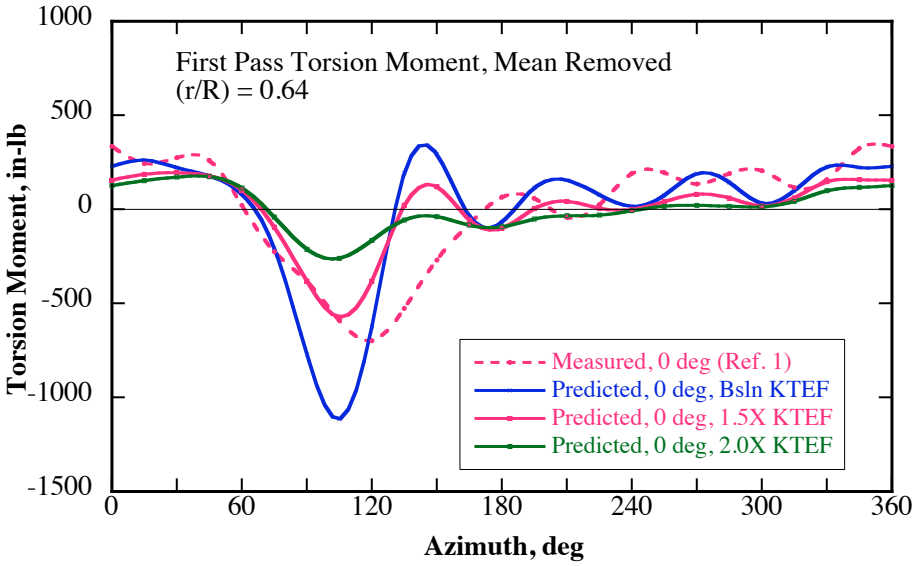

Fig. 2a. First pass torsion moment correlation at 0.64R, flap hinge stiffness effect, $\mu = 0.3$, $C_T/\sigma = 0.08$, $\alpha_s = -9.1$ deg.

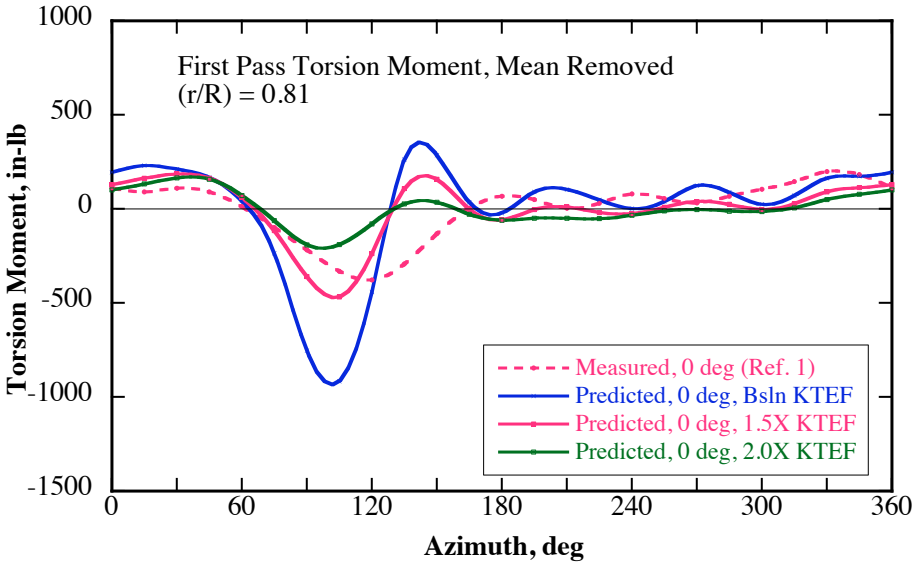

Fig. 2b. First pass torsion moment correlation at 0.81R, flap hinge stiffness effect, $\mu = 0.3$, $C_T/\sigma = 0.08$, $\alpha_s = -9.1$ deg.

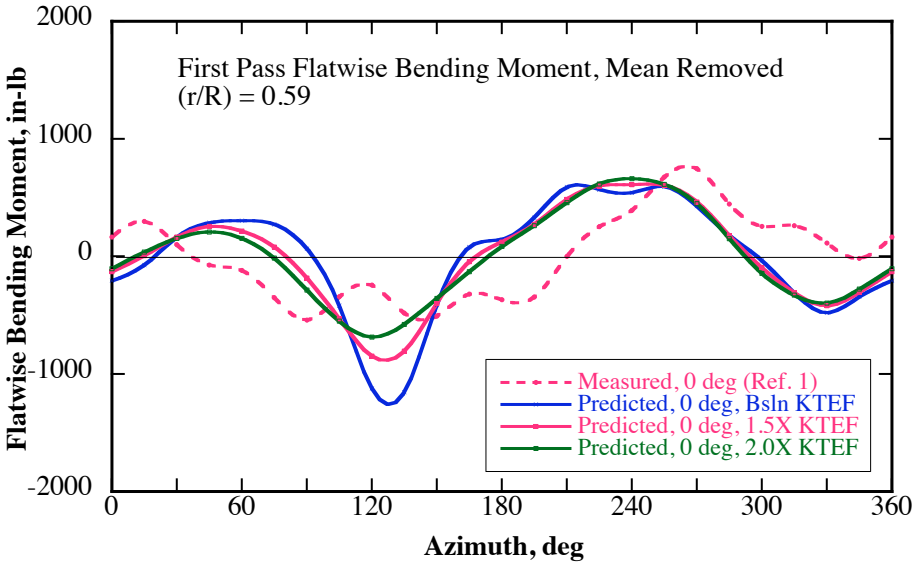

Fig. 2c. First pass flatwise bending moment correlation at 0.59R, flap hinge stiffness effect, $\mu = 0.3$, $C_T/\sigma = 0.08$, $\alpha_s = -9.1$ deg.

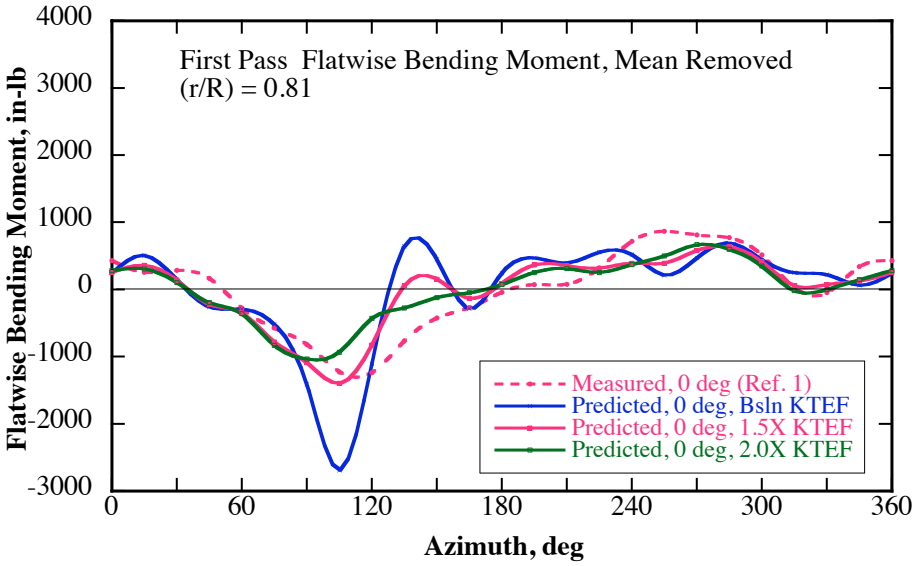

Fig. 2d. First pass flatwise bending moment correlation at 0.81R, flap hinge stiffness effect, $\mu = 0.3$, $C_T/\sigma = 0.08$, $\alpha_s = -9.1$ deg.

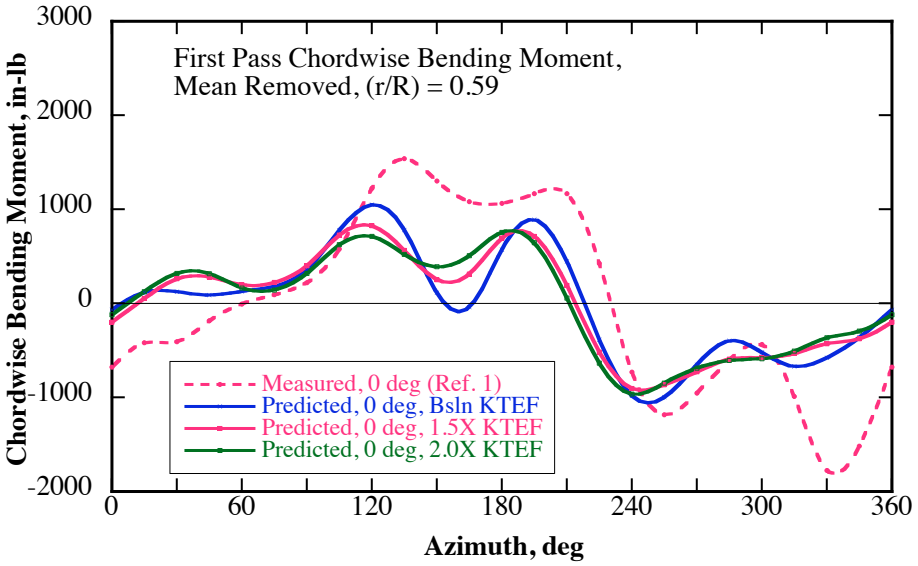

Fig. 2e. First pass chordwise bending moment correlation at 0.59R, flap hinge stiffness effect, $\mu = 0.3$, $C_T/\sigma = 0.08$, $\alpha_s = -9.1$ deg.

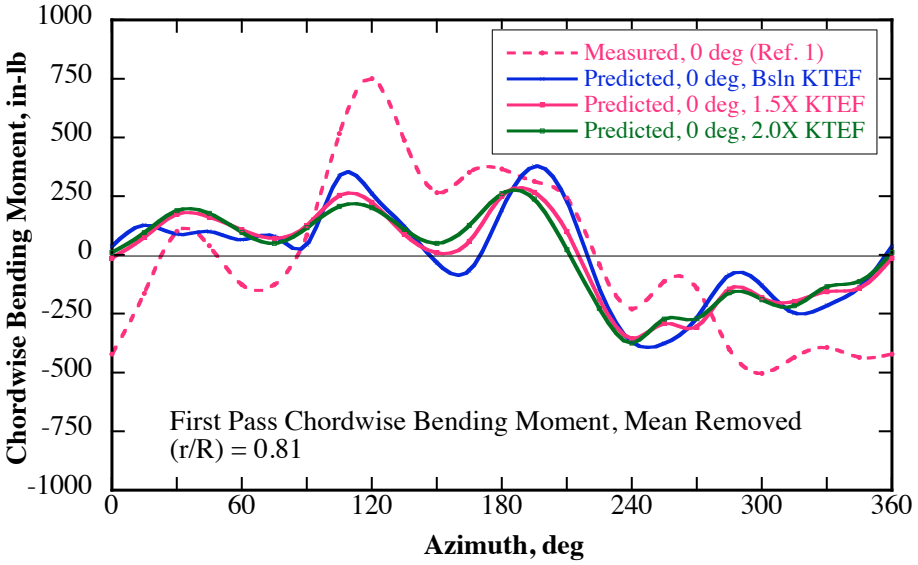

Fig. 2f. First pass chordwise bending moment correlation at 0.81R, flap hinge stiffness effect, $\mu = 0.3$, $C_T/\sigma = 0.08$, $\alpha_s = -9.1$ deg.

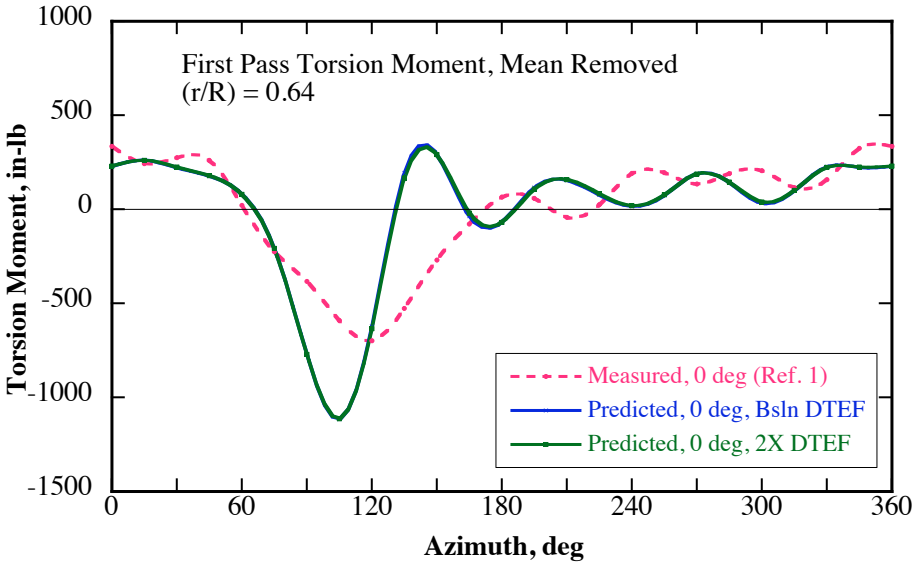

Fig. 2g. First pass torsion moment correlation at 0.64R, flap hinge damping effect, $\mu = 0.3$, $C_T/\sigma = 0.08$, $\alpha_s = -9.1$ deg.

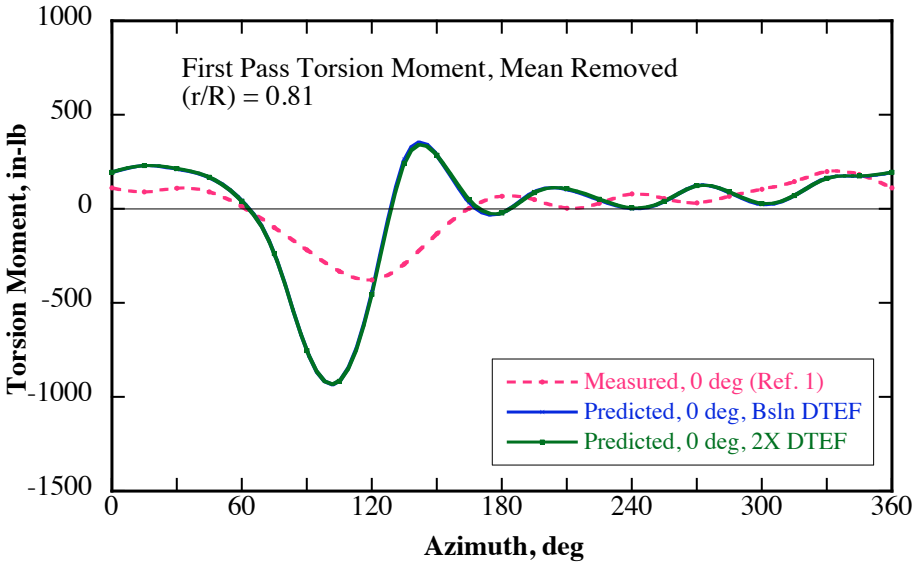

Fig. 2h. First pass torsion moment correlation at 0.81R, flap hinge damping effect, $\mu = 0.3$, $C_T/\sigma = 0.08$, $\alpha_s = -9.1$ deg.

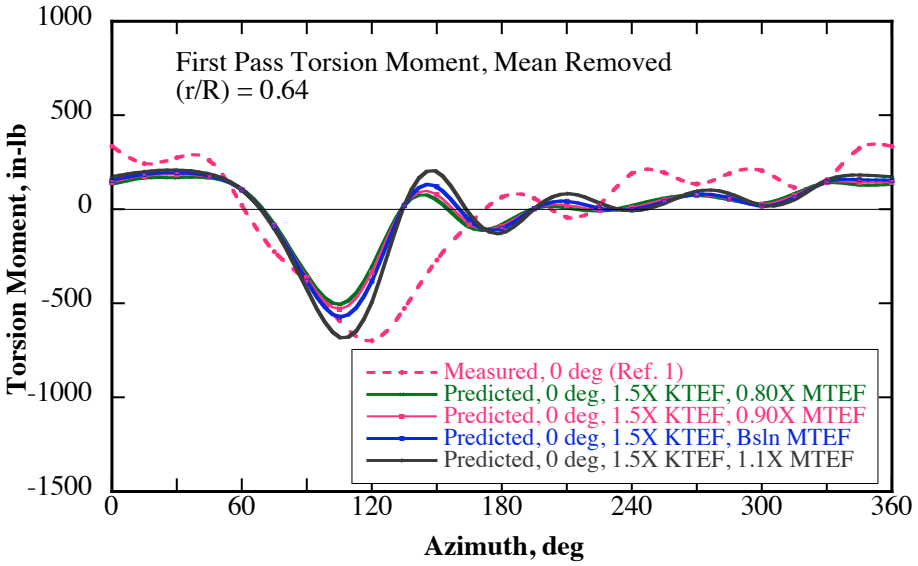

Fig. 2i. First pass torsion moment correlation at 0.64R, flap mass effect, $\mu = 0.3$, $C_T/\sigma = 0.08$, $\alpha_s = -9.1$ deg.

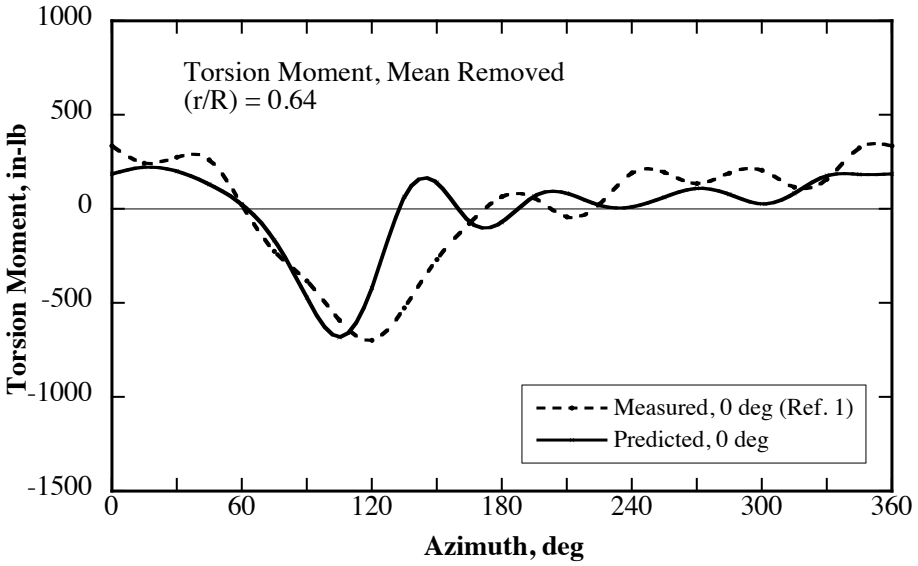

Fig. 3a. Torsion moment correlation at 0.64R, 0 deg flap deflection, $\mu = 0.3$, $C_T/\sigma = 0.08$, $\alpha_s = -9.1$ deg.

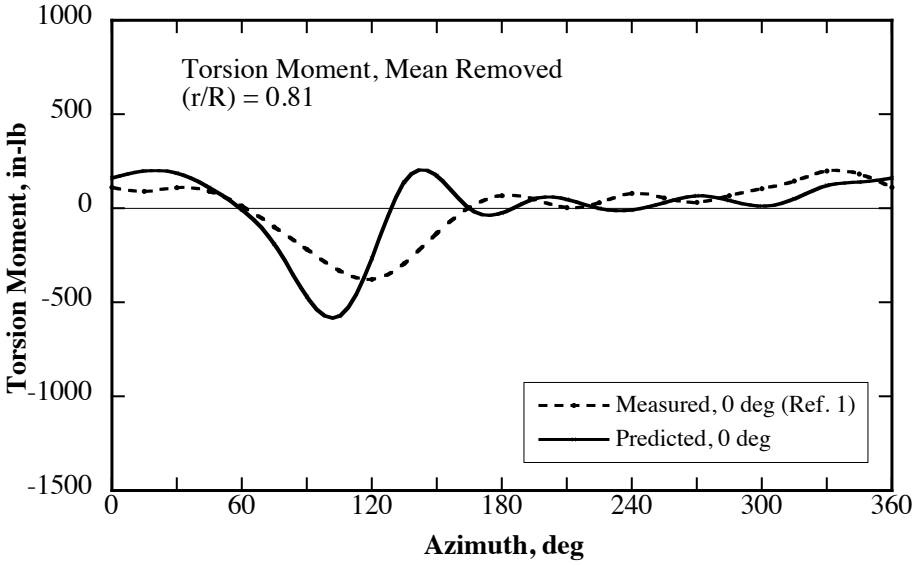

Fig. 3b. Torsion moment correlation at 0.81R, 0 deg flap deflection, $\mu = 0.3$, $C_T/\sigma = 0.08$, $\alpha_s = -9.1$ deg.

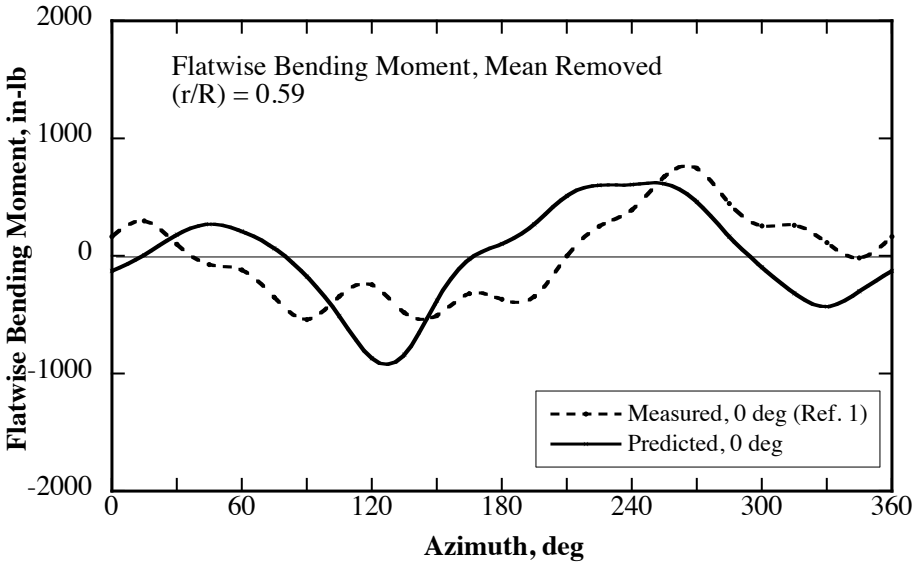

Fig. 3c. Flatwise bending moment correlation at 0.59R, 0 deg flap deflection, $\mu = 0.3$, $C_T/\sigma = 0.08$, $\alpha_s = -9.1$ deg.

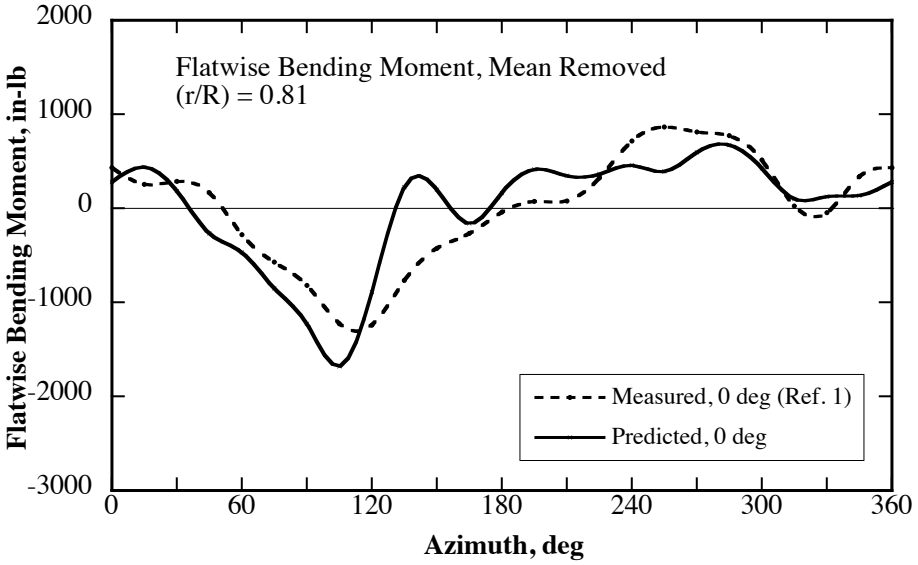

Fig. 3d. Flatwise bending moment correlation at 0.81R, 0 deg flap deflection, $\mu = 0.3$, $C_T/\sigma = 0.08$, $\alpha_s = -9.1$ deg.

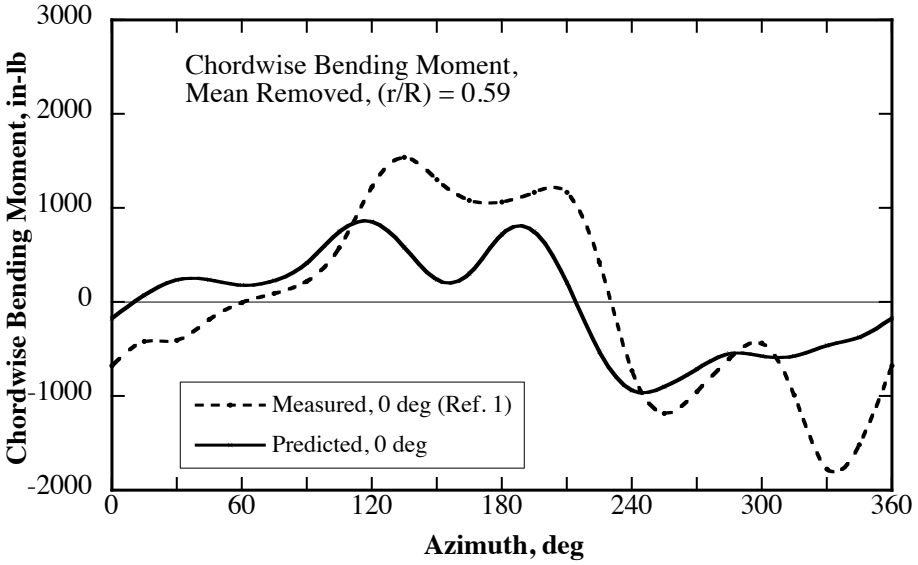

Fig. 3e. Chordwise bending moment correlation at 0.59R, 0 deg flap deflection, $\mu = 0.3$, $C_T/\sigma = 0.08$, $\alpha_s = -9.1$ deg.

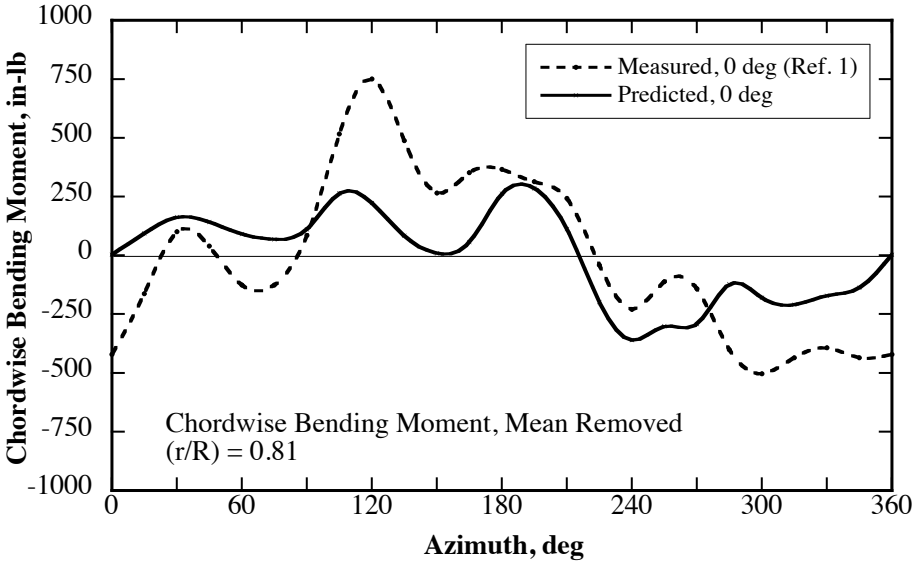

Fig. 3f. Chordwise bending moment correlation at 0.81R, 0 deg flap deflection, $\mu = 0.3$, $C_T/\sigma = 0.08$, $\alpha_s = -9.1$ deg.

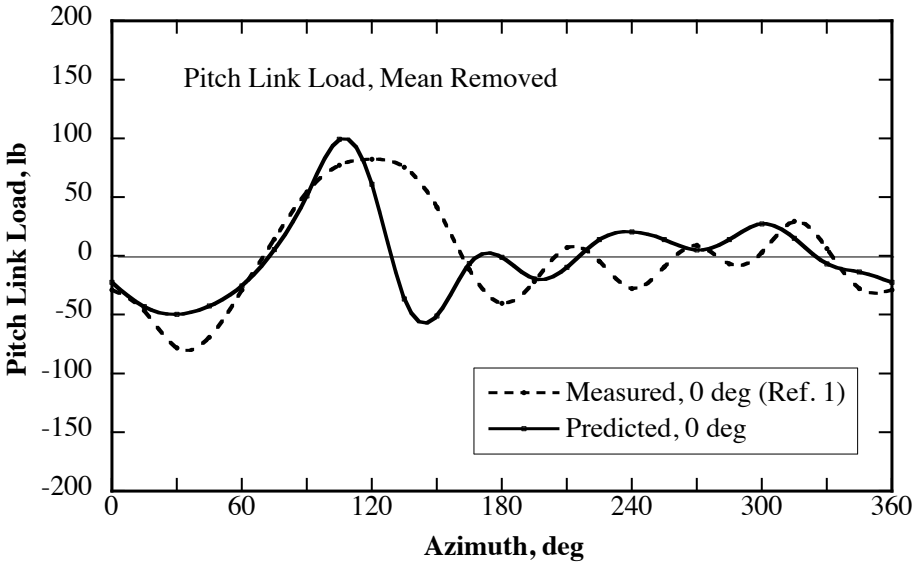

Fig. 4. Pitch link load correlation, 0 deg flap deflection, $\mu = 0.3$, $C_T/\sigma = 0.08$, $\alpha_s = -9.1$ deg.

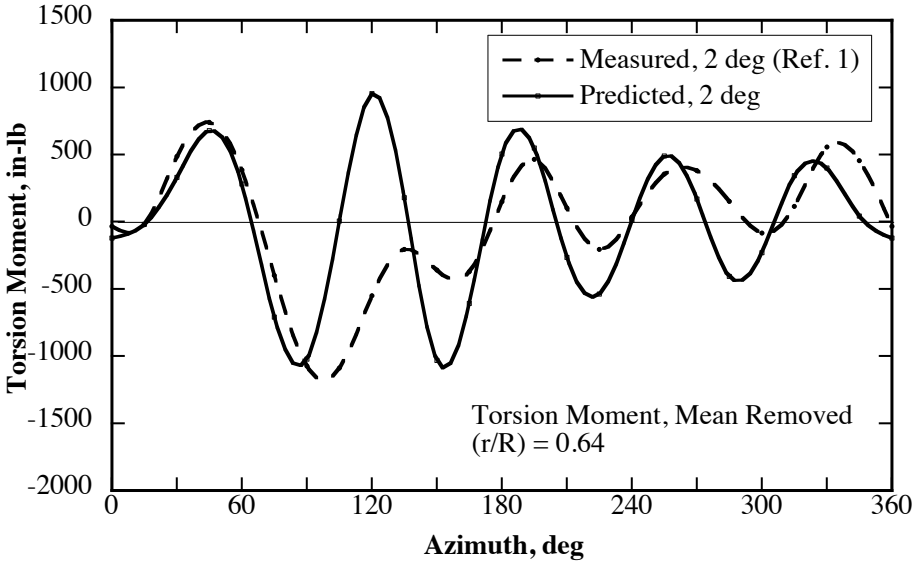

Fig. 5a. Torsion moment correlation at 0.64R, 5P, 2 deg flap deflection, $\mu = 0.3$, $C_T/\sigma = 0.08$, $\alpha_s = -9.1$ deg.

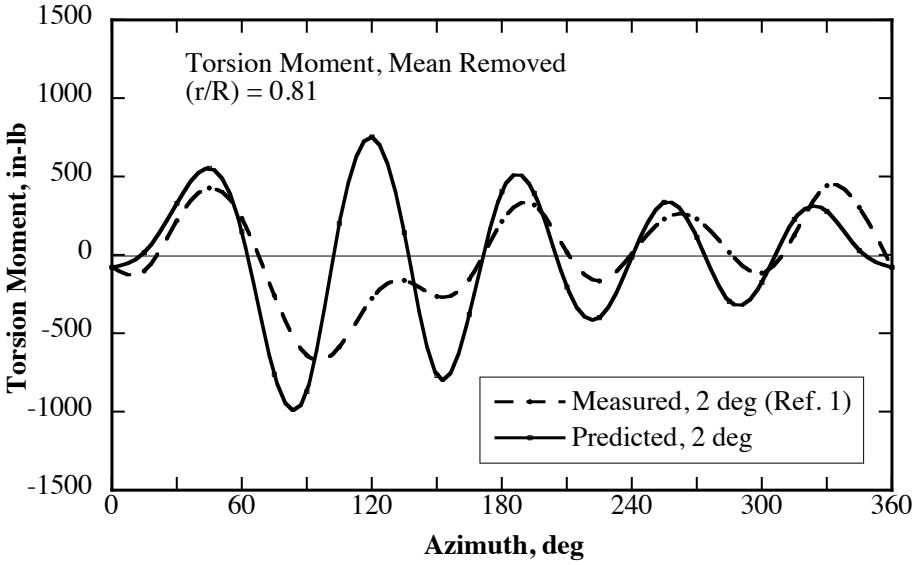

Fig. 5b. Torsion moment correlation at 0.81R, 5P, 2 deg flap deflection, $\mu = 0.3$, $C_T/\sigma = 0.08$, $\alpha_s = -9.1$ deg.

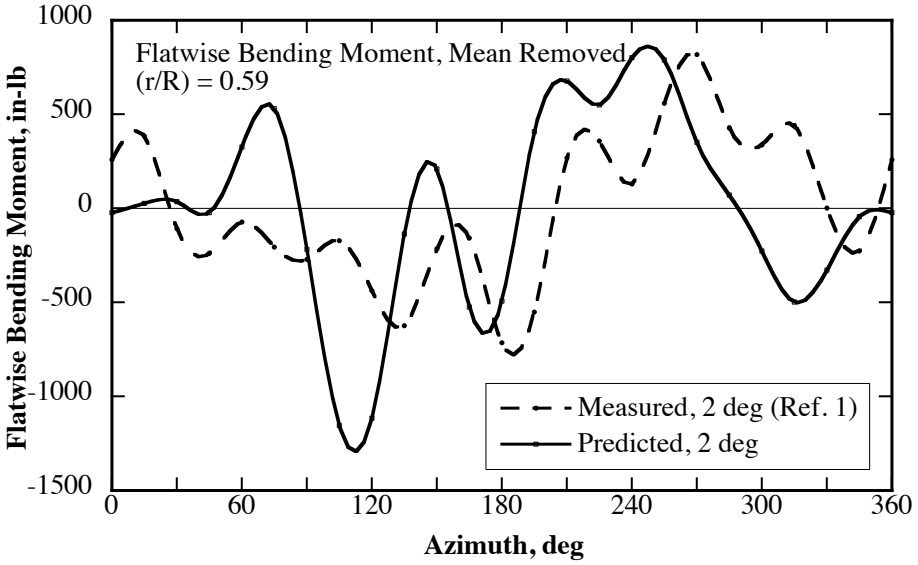

Fig. 5c. Flatwise bending moment correlation at 0.59R, 5P, 2 deg flap deflection, $\mu = 0.3$, $C_T/\sigma = 0.08$, $\alpha_s = -9.1$deg.

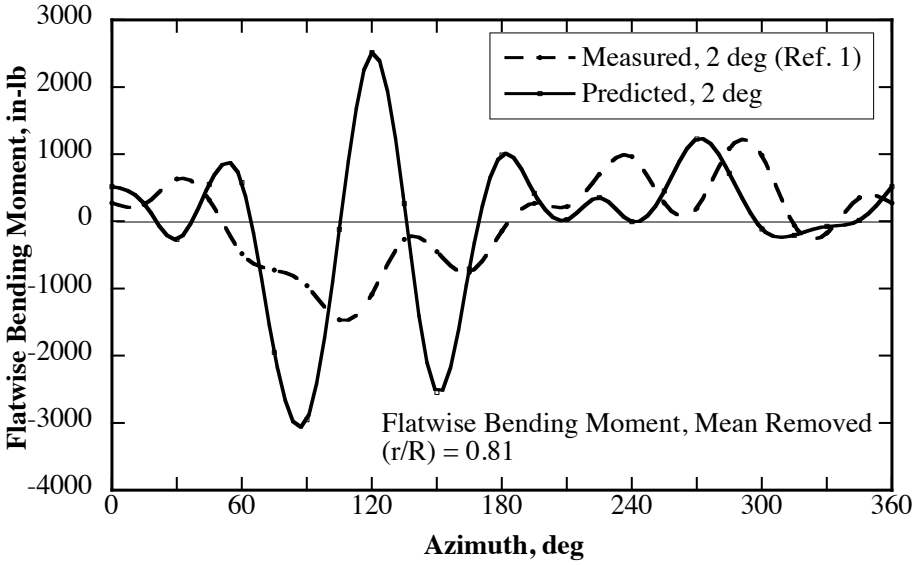

Fig. 5d. Flatwise bending moment correlation at 0.81R, 5P, 2 deg flap deflection, $\mu = 0.3$, $C_T/\sigma = 0.08$, $\alpha_s = -9.1$ deg.

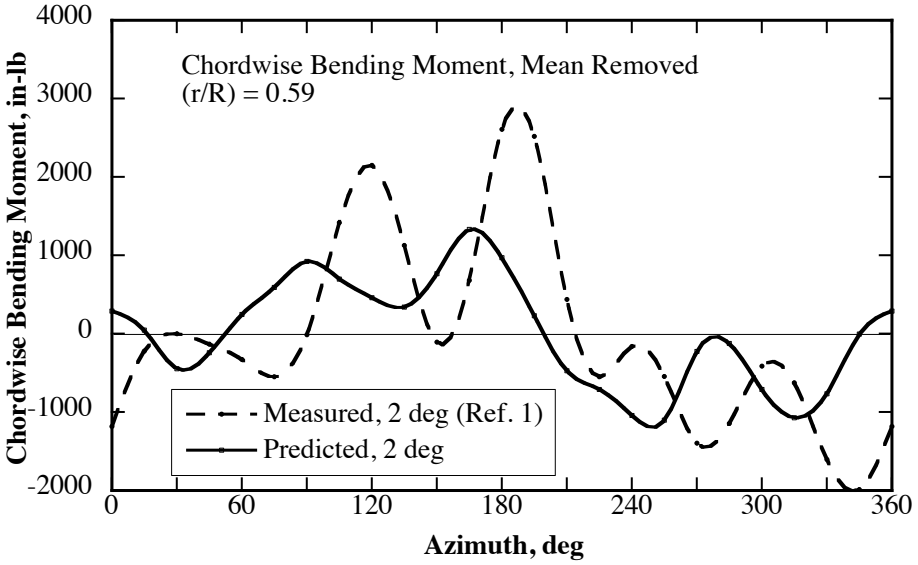

Fig. 5e. Chordwise bending moment correlation at 0.59R, 5P, 2 deg flap deflection, $\mu = 0.3$, $C_T/\sigma = 0.08$, $\alpha_s = -9.1$ deg.

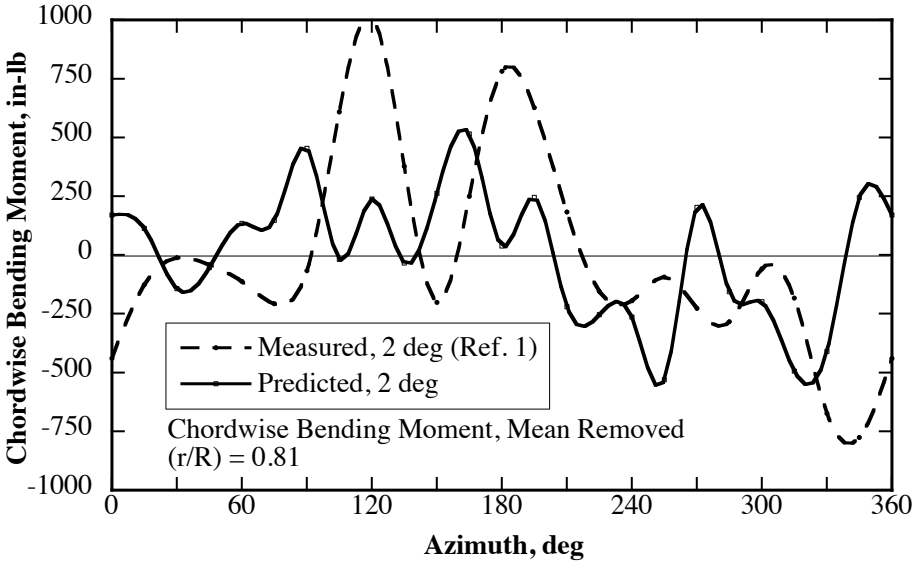

Fig. 5f. Chordwise bending moment correlation at 0.81R, 5P, 2 deg flap deflection, $\mu = 0.3$, $C_T/\sigma = 0.08$, $\alpha_s = -9.1$ deg.

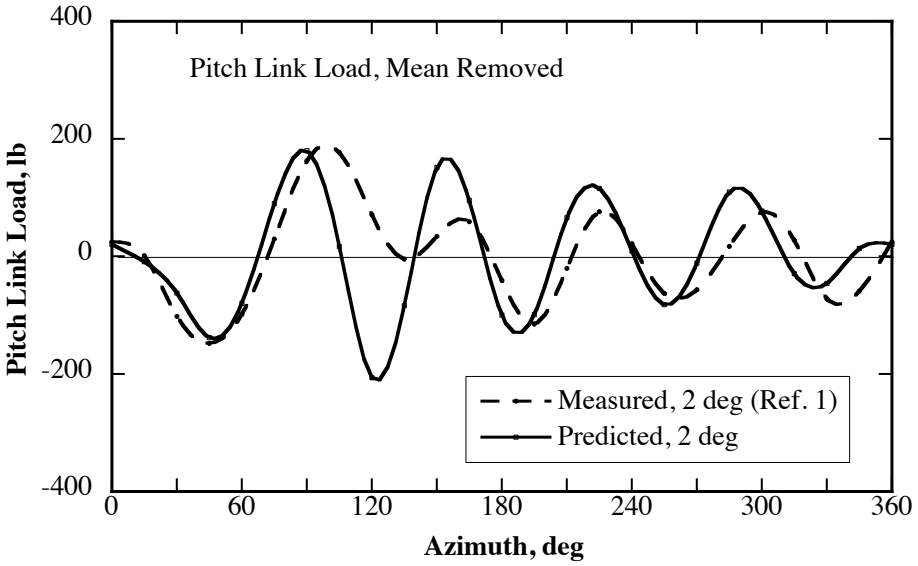

Fig. 6. Pitch link load correlation, 5P, 2 deg flap deflection, $\mu = 0.3$, $C_T/\sigma = 0.08$, $\alpha_s = -9.1$ deg.

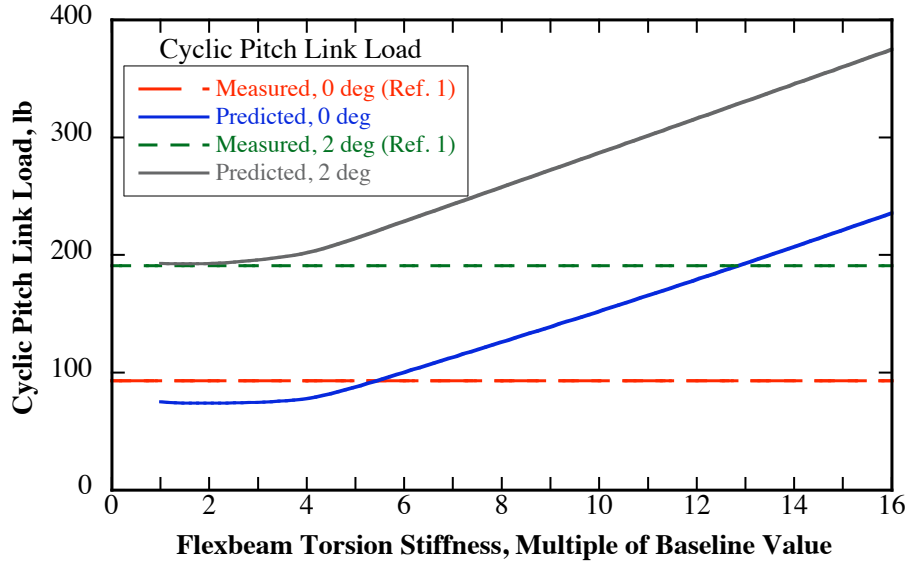

Fig. 7. Predicted effect of flexbeam torsion stiffness on the cyclic pitch link load, $\mu = 0.3$, $C_T/\sigma = 0.08$, $\alpha_s = -9.1$ deg.